

Magnetic plateaus and jumps in a spin-1/2 ladder with alternate Ising-Heisenberg rungs: a field dependent study

Sk Saniur Rahaman¹

Manoranjan Kumar^{1,§}

Shaon Sahoo^{2,§}

E-mail: manoranjan.kumar@bose.res.in

E-mail: shaon@iittp.ac.in

§

¹ S. N. Bose National Centre for Basic Sciences, Block JD, Sector III, Salt Lake, Kolkata 700106, India

² Department of Physics, Indian Institute of Technology, Tirupati, India

Abstract. We study a frustrated two-leg spin-1/2 ladder with alternate Ising and isotropic Heisenberg rung exchange interactions, whereas, interactions along legs and diagonals are Ising type. The ground-state (GS) of this model has four exotic phases: (i) the stripe rung ferromagnet (SRFM), (ii) the anisotropic anti-ferromagnet (AAFm), (iii) the Dimer, and (iv) the stripe leg ferromagnet (SLFM) in absence of any external magnetic field. In this work, we study the effect of externally applied longitudinal and transverse fields on GS phases and note that there are two plateaus with per-site magnetization 1/4 and 1/2. There is another plateau at zero magnetization due to a finite spin gap in the presence of a longitudinal field. The exact diagonalization (ED) and the transfer matrix (TM) methods are used to solve the model Hamiltonian and the mechanism of plateau formation is analyzed using spin density, quantum fidelity, and quantum concurrence. In the (i) SRFM phase, Ising exchanges are dominant for all spins but the Heisenberg rungs are weak, and therefore, the magnetization shows a continuous transition as a function of the transverse field. In the other three phases [(ii)-(iv)], the Ising dimer rungs are weak and those are broken first to reach a plateau with per-site magnetization 1/4, having a large gap which is closed by further application of the transverse field.

§ The last two authors have equal contributions.

1. Introduction

Frustrated low-dimensional quantum magnets exhibit a diverse range of quantum phases that generate significant interest among both theorists and experimentalists. Consequently, theoretical studies are crucial for verifying experimental results, especially due to the continuous synthesis of low-dimensional magnetic materials [1–15]. In the spin chains and ladder systems, the competing exchange interactions lead to many interesting quantum phases like ferromagnetic ground state (GS) [16], Néel phase [17–19], Luttinger liquid [20, 21], spiral [22], spin liquid [23, 24], dimer phase [4], etc. The antiferromagnetic isotropic Heisenberg spin-1/2 zigzag ladder or the $J_1 - J_2$ chain has a gapless spectrum in strong leg coupling limit, whereas, it has a gapped spectrum for the moderate value of the ratio of the exchange interactions due to dimerization along the rung. [25–31].

The anisotropy in the exchange interaction significantly influences the GS properties. For example, the isotropic Heisenberg spin-1/2 $J_1 - J_2$ model in the small J_2 limit has a gapless spectrum and its GS is a spin liquid phase with quasi-long range order (QLRO) [25, 29, 30]. But, the spectrum of the XXZ Heisenberg spin-1/2 chain is gapped for a large axial anisotropy $\Delta > 1$, and in this limit, the spins behave like Ising type, whereas, the spectrum is gapless for $\Delta < 1$ and spins are aligned in XY plane [32, 33]. The GS of an isotropic Heisenberg spin-1/2 normal ladder exhibits short range order and the spin gap is finite for any non-zero value of rung exchange. On the other hand, the spectrum of the anisotropic ladder systems can be gapless [33–39]. In a spin-1/2 ladder with isotropic rung and axial anisotropic leg exchange Δ , the GS can be tuned from singlet to Néel phase by increasing Δ [36]. But, for a normal spin-1/2 ladder with anisotropy in both leg and rung exchange interactions, the GS can be XY, Néel, or rung singlet (RS) phase on tuning the rung exchange and axial anisotropy [38]. Another type of anisotropic spin-1/2 ladder is the Kitaev-Heisenberg model on a two-leg ladder where the GS has many exotic quantum phases [39].

Many spin-1/2 ladders with isotropic and anisotropic exchange interactions are reported to display magnetic plateaus and jumps in the magnetization curve by tuning the external magnetic field [40–54]. Japaridze et al. studied a two-leg spin- $\frac{1}{2}$ ladder sys-

tem with leg interaction J_{\parallel} and alternate rung as J_{\perp}^+ , J_{\perp}^- in presence of a longitudinal field h , and show that the system have zero magnetization plateau up to h_{c1}^- , a plateau at half of the saturation magnetization for the magnetic field between h_{c1}^+ and h_{c2}^- and fully polarized spin is achieved at h_{c2}^+ [45]. Moradmard et al. studied a spin-1/2 ladder system with XXZ interaction and they showed different phases like x-FM, z-FM, y-Néel, and z-Néel in a magnetic phase diagram in the plane of anisotropy interaction Δ and magnetic field h [46]. Similarly, Dey et.al. carried out the magnetization study of isotropic Heisenberg spin-1/2 on a 5/7-skewed ladder and showed multiple plateau phases with field h [47]. They also note that plateau phases are the consequences of gaps in the spectrum, and these plateau phases can be explained in terms of Oshikawa, Yamanaka, and Affleck (OYA) criterion [48].

Some of the real compounds like the heterobimetallic coordination polymer $[(Tp)_2Fe_2(CN)_6(OAc)(bap)Cu_2(CH_3OH)_2CH_3OH \cdot H_2O]$ forms an effective Ising-Heisenberg spin-1/2 branched chain model [51], whereas, $(VO)_2P_2O_7$, CaV_2O_5 and MgV_2O_5 can be modeled by using two legs spin-1/2 ladders with the Ising-Heisenberg exchange [52]. The quantum phase diagram, magnetization curves, and concurrence of the spin-1/2 Ising Heisenberg branched chain are studied using the transfer-matrix method and they note the plateau at 1/2 of saturation magnetization [51]. For a two-leg spin-1/2 ladder with Ising exchange along the leg, diagonal, and Heisenberg exchange along the rung, Verkholyak et. al. noted that on applying a longitudinal magnetic field, the Néel phase of the GS undergoes a phase transition to a half plateau or staggered bond (SB) phase in presence of moderate field and to a fully spin-polarized state for strong field limit [52]. With few similarities to these ladder systems, we propose another type of anisotropic spin-1/2 two-leg ladder which may have various types of plateau at 0, 1/2, and full of saturation magnetization. The quantum phase transition in these systems can alternatively be determined using the concurrence [55, 56] and fidelity [57] calculations.

We consider a spin-1/2 frustrated two-leg ladder system with alternating Ising and Heisenberg type rung exchanges, where the diagonal and leg exchange are of Ising type as shown in Fig.1.a. In this model, J_c and J_q are the alternate Ising and Heisenberg rung exchange interactions respectively, where, J_{cq} and J_d are the leg and diagonal exchange interaction strengths

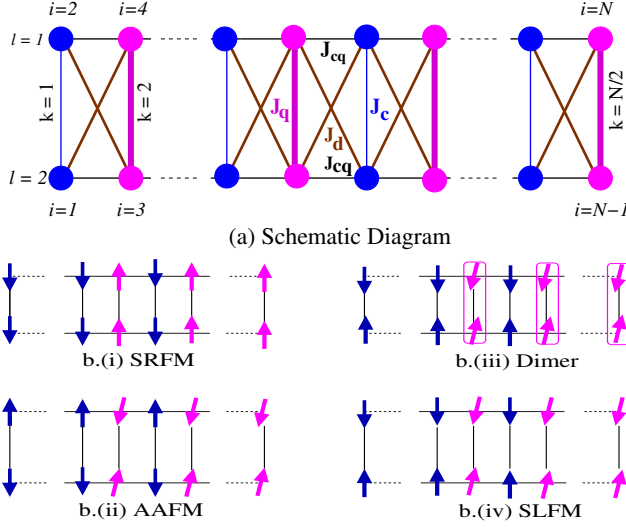


Figure 1. (color online) (a) Schematic diagram of the spin ladder with alternate Ising-Heisenberg rung interactions. J_c and J_q are the alternative Ising and Heisenberg type rung interactions respectively. J_{cq} , J_d are the Ising type leg and diagonal exchange interactions respectively. Blue and magenta color circles represent σ and S spins in Eq.1 respectively. l , k , and i represent leg and rung, and site indices respectively. The spin configurations of four exotic phases with $J_c = J_{cq} = 1$: b.(i) SRFM ($J_q = 0.2$, $J_d = 2.0$), b.(ii) AAFM ($J_q = 2.0$, $J_d = 0.4$), b.(iii) Dimer ($J_q = 2.0$, $J_d = 1.0$), and b.(iv) SLFM ($J_q = 2.0$, $J_d = 1.6$) are shown. Blue and magenta rung pairs are representing $\sigma - \sigma$ and $S - S$ rung pairs. The boxes shown in Subfigure b.(iii) represent perfect singlets. Quantum phases are studied earlier in Ref. [58].

of Ising type respectively. The quantum phase diagram of this model is studied earlier in parameter space of J_q and J_d (both are antiferromagnetic) by considering $J_c = J_{cq} = 1$ [58]. The system exhibits four distinct GS phases under periodic boundary condition (PBC): (i) stripe rung ferromagnet (SRFM), (ii) the anisotropic antiferromagnet (AAFM), (iii) the Dimer, and (iv) the stripe leg ferromagnet (SLFM) depending upon the values of J_q and J_d in absence of any magnetic field [58]. The GS phases are schematically represented in Fig1.b.[(i)-(iv)]. The SRFM phase is Ising dominated where all the spins are aligned along the z direction completely. Whereas, the [(ii)-(iv)] phases are anisotropic. Although all the rungs are antiferromagnetically aligned for the [(ii)-(iv)] phases, the spin arrangements along the leg are different. Along the leg, the alignment of the spins is anti-ferromagnetic for the AAFM phase and ferromagnetic for the SLFM phase. In the Dimer phase, there is no spin alignment along the leg. In this manuscript, we study the effect of both longitudinal and transverse magnetic fields on the four GS phases with a few sets of J_q , J_d values discussed in Sec.4.

In this work, we observe that in all the quantum phases, the system exhibits a plateau at 0, 1/2, and

1 of saturation magnetization in the presence of an externally applied longitudinal magnetic field. The calculations are done using the exact diagonalization (ED) [59] and transfer matrix (TM) [60] methods, and results from both methods agree excellently with each other. Furthermore, we calculate the zero-temperature limit quantum fidelity, fidelity susceptibility, and quantum concurrence from the partition function of the ladder using TM, and find that these results are in accordance with the exact calculation. The study of the magnetization under a transverse field is carried out using ED only, and it is noticed that the magnetization shows a half, and full of saturation magnetization plateaus.

This paper is divided into a few sections as follows. First, the model is discussed briefly in Sec. 2. This is followed by a discussion on methods in Sec. 3. In Sec. 4.1.1, the magnetization process is discussed in the presence of the longitudinal field. In Sec. 4.1.2 we discuss the zero-temperature limit quantum fidelity and bipartite concurrence for different phases. In Sec. 4.1.3, the quantum phase diagrams are shown for four different longitudinal fields. In Sec. 4.2, we discuss the magnetization process in the presence of a transverse field. In Sec. 5, we summarise the results and conclude the paper.

2. Model Hamiltonian

We construct the Hamiltonian for a spin-1/2 two-leg ladder with N number of spins periodically connected along the leg, which turns out to be comprised of $n = \frac{N}{4}$ number of unit cells. In each unit cell, one rung pair is connected through an Ising type exchange J_c , whereas, the other one is coupled with a Heisenberg type exchange J_q as shown in Fig.1.(a). These rungs couple each other through Ising type exchanges: J_{cq} along the leg, J_d along the diagonal. The spins with rung coupling J_c and J_q are marked with σ and \vec{S} respectively. Here onward, the Ising type and Heisenberg type rung spin pairs are to be called $\sigma - \sigma$ and $S - S$ pairs respectively. Let us now write down the Hamiltonian for the j^{th} unit cell as

$$\begin{aligned} \mathbf{H}_j = & J_q^z S_{2j,1}^z S_{2j,2}^z + \frac{J_q^{xy}}{2} \left[S_{2j,1}^+ S_{2j,2}^- + S_{2j,1}^- S_{2j,2}^+ \right] \\ & + \frac{J_c}{2} \left[\sigma_{2j-1,1} \sigma_{2j-1,2} + \sigma_{2j+1,1} \sigma_{2j+1,2} \right] + J_{cq} \times \\ & \left[S_{2j,1}^z (\sigma_{2j-1,1} + \sigma_{2j+1,1}) + S_{2j,2}^z (\sigma_{2j-1,2} + \sigma_{2j+1,2}) \right] \\ & + J_d \times \\ & \left[S_{2j,1}^z (\sigma_{2j-1,2} + \sigma_{2j+1,2}) + S_{2j,2}^z (\sigma_{2j-1,1} + \sigma_{2j+1,1}) \right] \end{aligned}$$

$$\begin{aligned}
& -\frac{h}{2} \sum_{l=1}^2 (2S_{2j,l}^z + \sigma_{2j-1,l} + \sigma_{2j+1,l}) \\
& -\frac{h^x}{2} \sum_{l=1}^2 (2S_{2j,l}^x + \sigma_{2j-1,l}^x + \sigma_{2j+1,l}^x)
\end{aligned} \quad (1)$$

Here, h and h^x are the longitudinal (+z direction) and transverse (+x direction) fields respectively. S^x , S^z are the spin components along +x, +z respectively of the spin \vec{S} , whereas, S^+ , S^- are the raising and lowering operators respectively of the same. In Eq.1, we consider $J_c = J_{cq} = 1$ and $J_q^z = J_q^{xy} = J_q$ throughout our manuscript. The general Hamiltonian of the ladder under PBC with system size N is the summation of the n unit cells, which can be written as $\mathbf{H} = \sum_{j=1}^n \mathbf{H}_j$.

3. Methods

We employ the ED method to solve the energy eigenvalues and eigenvectors of the Hamiltonian in Eq.1 for the system sizes $N = 16, 20, 24$ in the presence of longitudinal and transverse fields both. Whereas, in the absence of a transverse field i.e., for $h^x = 0$, the Hamiltonian of two consecutive units commute to each other, and so we employ the TM method to calculate the magnetization, quantum fidelity, quantum concurrence from free energy, and partition function. The partition function for the entire ladder with system size N (or $n = N/4$ unit) can be written as $Q_N(h, \beta) = \text{Tr}(e^{-\beta\mathbf{H}}) = [Q_4(h, \beta)]^n$ (see Appendix 7). $Q_4(h, \beta)$ is the partition function for one unit of 4 spins and β is the inverse temperature. For this model, $Q_N(h, \beta) = [\lambda_1^n + \lambda_2^n + \lambda_3^n + \lambda_4^n]$, where, $\lambda_1, \lambda_2, \lambda_3, \lambda_4$ are the eigenvalues of a 4×4 transfer matrix for one unit (see Appendix 7). In the limit $n \rightarrow \infty$, and with the condition $\lambda_1 \gg \lambda_2 \gg \lambda_3 \gg \lambda_4$, one can write $Q_N(h, \beta) \approx \lambda_1^n$ and $Q_4(h, \beta) \approx \lambda_1$. At zero-temperature limit i.e., for $\beta \rightarrow \infty$, after defining some of the system parameters: $\Delta_2 = \sqrt{1 + 4(\frac{1-J_d}{J_q^{xy}})^2}$, $Q = e^{\beta J_q^z/4}$, we obtain the partition function for one unit (from the Eq. 34 in Appendix 7)

$$\begin{aligned}
Q_4(h, \beta) = & 2e^{\frac{\beta(J_c)}{4}} \times \\
& [2Q^{-1} \text{Cosh}[\beta h] + Q \text{Cosh}[\frac{\beta J_q^{xy}}{2}] + Q \text{Cosh}[\frac{\beta J_q^{xy} \Delta_2}{2}]] \\
& + 2e^{\frac{-\beta(J_c - 4h)}{4}} \times \\
& \left[Q^{-1} \text{Cosh}[\beta(h - (J_{cq} + J_d))] + Q \text{Cosh}[\frac{\beta J_q^{xy}}{2}] \right] \quad (2)
\end{aligned}$$

For the simplicity, we rewrite the $Q_4(h, \beta)$ as a polynomial function of $e^{\beta h}$ as

$$Q_4(h, \beta) = a_0 e^{2\beta h} + b_0 e^{\beta h} + d_0 \quad (3)$$

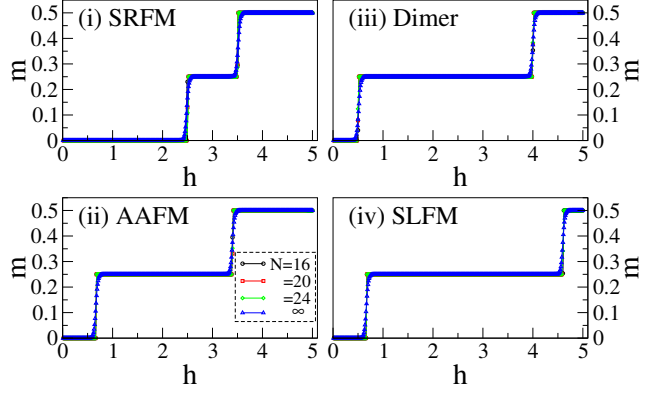


Figure 2. (PBC) Black, red, and green colors are the magnetization per site in the presence of a longitudinal field h for the system sizes $N = 16, 20, 24$ using ED. The blue color represents the magnetization calculated using the TM method at $T/J_c \rightarrow 0$. The values of J_q, J_d are (i) 0.2, 2.0 for the SRFM, (ii) 2.0, 0.4 for the AAFM, (iii) 2.0, 1.0 for the Dimer, and (iv) 2.0, 1.6 for the SLFM phases respectively.

Here, the system parameters a_0, b_0, d_0 are defined as

$$\begin{aligned}
a_0 &= e^{-\frac{\beta}{4}(J_q^z + J_c + 4J_{cq} + 4J_d)}, \\
b_0 &= 2e^{\frac{\beta}{4}(J_q^z - J_c)} \text{Cosh}[\frac{\beta J_q^{xy}}{2}] + 4e^{-\frac{\beta}{4}(J_q^z - J_c)}, \\
d_0 &= 2e^{\frac{\beta(J_q^z + J_c)}{4}} \left[\text{Cosh}[\frac{\beta J_q^{xy}}{2}] + \text{Cosh}[\frac{\beta J_q^{xy} \Delta_2}{2}] \right] \\
&+ e^{-\frac{\beta}{4}(J_q^z + J_c - 4J_{cq} - 4J_d)}. \quad (4)
\end{aligned}$$

4. Results

We study the magnetization properties in the presence of a longitudinal (h) and transverse (h^x) magnetic field in Sec.4.1 and Sec.4.2 respectively. In both of these cases, the studies are done for four sets of exchange parameters: (i) $J_q = 0.2, J_d = 2.0$ for the SRFM, (ii) $J_q = 2.0, J_d = 0.4$ for the AAFM, (iii) $J_q = 2.0, J_d = 1.0$ for the Dimer, and (iv) $J_q = 2.0, J_d = 1.6$ for the SLFM phases. It is to be mentioned that in all these cases, we consider J_c and J_{cq} to be unity.

4.1. Magnetization process in the presence of a longitudinal magnetic field

4.1.1. Magnetization vs field We obtain the per-site magnetization m for a finite system size N by calculating the spin gap i.e., the difference between the low-lying states of two different spin S^z sectors using ED. In Fig.2.[(i)-(iv)], we show the finite size scaling of the $m-h$ curve for three system sizes $N = 16, 20, 24$ using ED. $m-h$ curve shows three plateau phases: $m = 0, 1/4$, and $1/2$ connected by two magnetic jumps in each of the subfigures. The first jump is at h_{c1} from $m = 0$ to $1/4$, and the other at h_{c2} from $m = 1/4$ to full saturation of magnetization ($m = 1/2$) in all

four quantum phases as shown in Fig.2[(i)-(iv)]. The h_{c1} takes values 2.5, 0.7, 0.5, and 0.7, whereas, h_{c2} are 3.5, 3.5, 4, 4.5 for (i) the SRFM, (ii) the AAFM, (iii) the Dimer, and (iv) the SLFM phases respectively. Later on, we discuss in detail that these magnetic transitions show plateaus due to the spin gap and these jumps correspond to the overlap of the plateaus by unbinding of the rung dimers of equal energy. In all of the magnetization curves, it is noticed that there is a negligible finite-size effect. This is also noticed in the thermodynamic limit ($N \rightarrow \infty$) for the zero-temperature case ($\beta \rightarrow \infty$) using TM method.

Using the TM method, the per-site magnetization is obtained as $m = -\frac{1}{4} \frac{\partial F(h, \beta)}{\partial h}$, where $F(h, \beta)$ is the free energy for one unit and can be defined as $F(h, \beta) = -\frac{1}{\beta} \ln[Q_4(h, \beta)]$. The per-site magnetization in general can be written as

$$m = \frac{1}{4} \times \frac{[2a_0 e^{2\beta h} + b_0 e^{\beta h}]}{[a_0 e^{2\beta h} + b_0 e^{\beta h} + d_0]} \quad (5)$$

From the above equation, it is clear that the exponential terms compete and dominate each other in different limits of fields and m can take the discrete values $0, \frac{1}{4}, \frac{1}{2}$ (for $\beta \rightarrow \infty$). These magnetization plateaus can be connected by a few jumps which are associated with the critical fields and these critical fields are the mid-points of the jumps. At two critical fields h_{c1} and h_{c2} , m takes the values $\frac{1}{8}$ and $\frac{3}{8}$ respectively. However, the critical fields can be obtained from the Eq.5 as

$$h_{c1} \approx \frac{1}{\beta} \ln \left[\frac{d_0}{b_0} \right], h_{c2} \approx \frac{1}{\beta} \ln \left[\frac{b_0}{a_0} \right]. \quad (6)$$

These critical fields are found to match with the exact calculations discussed above and shown in the $m-h$ curve in Fig.2. Plateau width can be obtained as

$$d = |h_{c2} - h_{c1}| \approx \frac{1}{\beta} \ln \left[\frac{b_0^2}{a_0 d_0} \right] \quad (7)$$

From the above discussion one can conclude that in $\beta \rightarrow \infty$ limit, the partition function $Q_4(h, \beta)$ of Eq.3 can be simplified as following

$$Q_4(h, \beta) \approx \begin{cases} d_0 & \text{if } h \leq h_{c1} \\ b_0 e^{\beta h} & \text{if } h_{c1} \leq h \leq h_{c2} \\ a_0 e^{2\beta h} & \text{if } h \geq h_{c2} \end{cases} \quad (8)$$

Similarly, the free energy $F(h, \beta)$ can be written for three different plateau phases

$$F(h, \beta) = \begin{cases} -\frac{1}{\beta} \ln[d_0] & \text{if } h \leq h_{c1} \\ -\frac{1}{\beta} \ln[b_0] - h & \text{if } h_{c1} \leq h \leq h_{c2} \\ -\frac{1}{\beta} \ln[a_0] - 2h & \text{if } h \geq h_{c2} \end{cases} \quad (9)$$

From the above expressions of the free energy, it is noticed that the per-site magnetization can easily be

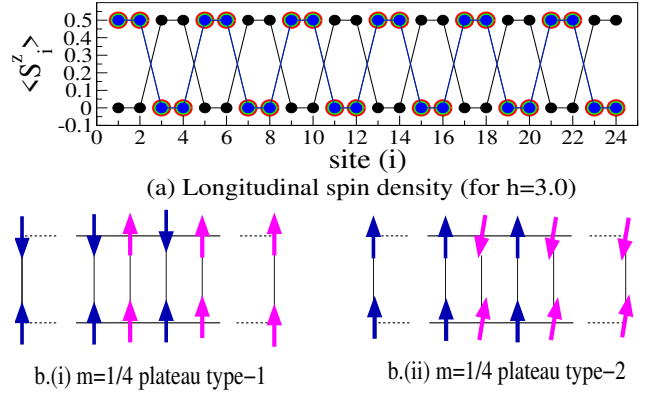


Figure 3. (a) Longitudinal spin density S_i^z is shown as a function of site index i for four GS phases: the SRFM ($J_q = 0.2, J_d = 2.0$), the AAFM ($J_q = 2.0, J_d = 0.4$), the Dimer ($J_q = 2.0, J_d = 1.0$), and the SLFM ($J_q = 2.0, J_d = 1.6$) using black, red, green, blue colors respectively. The spin configurations in b.(i) $m = 1/4$ plateau type-1, b.(ii) $m = 1/4$ plateau type-2 are shown. In $m = 1/4$ plateau type-1, all the Heisenberg rung pairs $S-S$ (magenta spins) are fully polarized, and in $m = 1/4$ plateau type-2, all the Ising rung pairs $\sigma-\sigma$ (blue spins) are fully polarized.

obtained from $m = -\frac{1}{4} \frac{\partial F(h, \beta)}{\partial h}$ to be $0, 1/4, 1/2$ for the three plateau phases. All of the four nonmagnetic GS phases (i.e., $m = 0$) have a finite magnetic excitation gap and it requires a finite external magnetic field h to reach a magnetic GS. The lowest magnetic excitation is in $m = 1/4$, for which the gap from the nonmagnetic GS is closed by a finite field h_{c1} . However, the $m = 1/4$ state has also a finite magnetic excitation gap and it requires a field h_{c2} to achieve the higher magnetic excitation $m = 1/2$, which is a fully polarized phase (FP). All the nonmagnetic GS ($m = 0$), $m = 1/4$ magnetic GS and $m = 1/2$ magnetic GS phases can be described by the system parameters d_0 , b_0 , and a_0 respectively.

To investigate the nature of all the plateau phases, spin density $\langle S_i^z \rangle$ at site i calculated using the ED is shown in Fig.3. (a). The SRFM phase is stabilized in the presence of the dominant diagonal Ising exchange whereas, in the other three phases isotropic Heisenberg rung exchange is dominant. Therefore, the formation of the $m = 1/4$ plateau from the SRFM phase (with low J_q and high J_d) is different from the other three phases. In the SRFM phase, the diagonal exchange J_d exhibits Ising characteristics and is stronger compared to the other exchanges. The formation of rung dimers and the dominant Ising exchange create a finite gap between the non-magnetic ($m = 0$) and magnetic ($m = 1/4$) phases. To close this gap and transition to the $m = 1/4$ plateau phase, a large field $h_{c1} = 2.5$ is required, as shown in Fig. 2. (i). At this critical field, the weakly coupled Heisenberg rung dimers ($S-S$) break down and get polarized, resulting in a finite spin density of 0.5, as depicted in Fig. 3.(a). The ground state

spin configuration for the $m = 1/4$ plateau is termed “ $m=1/4$ plateau type-1” or “P-I” and is shown in Fig. 3.b.(i). With further increase of the field around $h = 3.5$, all the spin pairs are broken and the system goes to the FP phase.

The AAFM, Dimer, and SLFM phases are characterized by strong Heisenberg rung exchange J_q , leading to the formation of strong dimers on $S-S$ pairs, which are energetically more stable compared to the dimers of $\sigma-\sigma$ pairs interacting with Ising exchange. In the AAFM phase, with anisotropic antiferromagnetic spin alignment on the ladder for $J_q = 2.0$ and $J_d = 0.4$, a very small field $h_{c1} = 0.7$ is sufficient to break the $\sigma-\sigma$ pairs and reach the $m = 1/4$ plateau, as shown in Fig.2.(ii). In the $m = 1/4$ plateau of AAFM, the rung spins of $\sigma-\sigma$ pairs are fully polarized with a spin density of 0.5, as depicted in Fig.3.(a). The spin configuration of this type of magnetic phase is referred to as “ $m=1/4$ plateau type-2” or “P-II” and is shown in Fig. 3.b.(ii).

In the Dimer phase, all the rung dimers are isolated, and the Ising dimers have a smaller spin gap as compared to the $S-S$ rung singlets. An external field of $h_{c1} = 0.5$ is sufficient to close the gap for a given value of $J_q = 2.0$ and $J_c = 1.0$ as shown in Fig.2.(iii). Due to the formation of perfect dimers through strong J_q exchange in this phase, the P-II phase exhibits a much larger gap, leading to a broader plateau width compared to the AAFM phase, as shown in Fig. 2.(iii). In the SLFM phase, the ground state exhibits ferromagnetic spin arrangements along the leg, while spins on different legs are oppositely aligned. Fig. 2.(iv) demonstrates that the onset of the P-II occurs at a field of $h_{c1} = 0.7$, with the largest plateau width observed in this phase. The spin density analysis reveals that the dimers formed by $\sigma-\sigma$ pairs become polarized along the field direction in the P-II phase as shown in Fig.3.b.(ii). Similar to the AAFM phase, the $\sigma-\sigma$ rung dimers are weaker in this phase also, while the oppositely aligned legs enhance the stability of singlets on the Heisenberg pair $S-S$, resulting in an extended plateau width. With further increase in the applied field, the P-II plateau as shown in Fig.3.b.(ii) is disrupted, and a sharp jump occurs at $h_{c2} = 4.5$ and reaches the FP plateau. In all four phases, either all $S-S$ or all $\sigma-\sigma$ rung pairs are simultaneously disrupted, leading to magnetic jumps.

4.1.2. Quantum Fidelity and Bipartite Concurrence

The spin arrangement of the plateau phases is quite different for all four phases at $h = 0$. Therefore, we expect the wave function of the plateau phases should be different and can be understood from the perspective of quantum information theory. In this subsection, we calculate and show the zero temperature

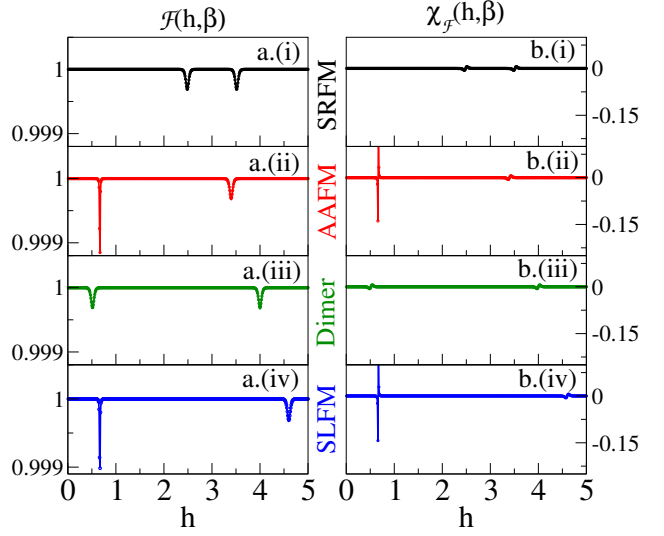


Figure 4. (a) (left column) Quantum fidelity $\mathcal{F}(h, \beta)$ and (b) (right column) fidelity susceptibility $\chi_{\mathcal{F}}(h, \beta)$ calculated using TM are shown for the thermodynamic limit ($N \rightarrow \infty$) at $T/J_c \rightarrow 0$. Black, red, green, and blue colors representing four phases: the SRFM ($J_q = 0.2, J_d = 2.0$), the AAFM ($J_q = 2.0, J_d = 0.4$), the Dimer ($J_q = 2.0, J_d = 1.0$), and the SLFM ($J_q = 2.0, J_d = 1.6$) respectively are arranged sequentially from top to bottom in both the columns.

limit quantum fidelity and bipartite concurrence to analyze the plateaus, and these can be obtained from the partition function as discussed below. Quantum fidelity is the measurement of overlap between two states and can be used to characterize the phase transition on the tuning of parameters. Quan et. al. have shown that fidelity can be obtained from the partition function [57]. Similarly, we calculate the quantum fidelity for the field h with small perturbation δh as:

$$\mathcal{F}(h, \beta) = \frac{Q_4(h, \beta)}{\sqrt{Q_4(h + \delta h, \beta)Q_4(h - \delta h, \beta)}} \quad (10)$$

where $Q_4(h, \beta)$ is the partition function for one unit cell in this case. $\mathcal{F}(h, \beta)$ is unity when there is a unique state and discontinuous at the phase transition points. The Field fidelity susceptibility $\chi_{\mathcal{F}}(h, \beta) = \frac{\partial \mathcal{F}(h, \beta)}{\partial h}$ is zero in unique state and it diverges at the transition. $\mathcal{F}(h, \beta)$ can further be written in terms of the free energy $F(h, \beta)$ and magnetic susceptibility $\chi(h, \beta)$ as

$$\begin{aligned} \mathcal{F}(h, \beta) &= e^{-\beta \left[F(h, \beta) - \frac{F(h - \delta h, \beta) + F(h + \delta h, \beta)}{2} \right]} \\ &\approx e^{-\left[\frac{(\beta \delta h)^2}{4} \chi(h, \beta) \right]} \end{aligned} \quad (11)$$

In the plateau phases, $\chi(h, \beta) = -\frac{\partial^2 F(h, \beta)}{\partial h^2} = \frac{\partial m}{\partial h}$ is zero and so the fidelity $\mathcal{F}(h, \beta)$ in Eq.11 is unity. On the other hand, at the magnetic jumps, the $\chi(h, \beta)$ diverges, and the $\mathcal{F}(h, \beta)$ decreases from unity.

Fig.4.a. [(i)-(iv)], and b. [(i)-(iv)] show the plot of $\mathcal{F}(h, \beta)$ (left column) and $\chi_{\mathcal{F}}(h, \beta)$ (right column) as

a function of h respectively for four different phases: (i) the SRFM, (ii) the AAFM, (iii) the Dimer, and (iv) the SLFM respectively. In each of the sub-figures of $\mathcal{F}(h, \beta)$ and $\chi(h, \beta)$, two discontinuities are noticed for all four phases. All of these discontinuities are consistent with the jumps of the $m - h$ curve in Fig.2 and represent the magnetic phase transitions.

We also calculate the bond order to understand the configurational change and bipartite concurrence to measure the quantum nature of the $S - S$ pair which is connected through a Heisenberg rung exchange J_q . If the concurrence has some finite value, the wavefunction is in a mixed or entangled state, otherwise, it is in a pure state if the concurrence is zero. Wothers et.al. and Karlova et. al. in their study calculate concurrence for a spin pair connected by Heisenberg interaction in terms of the local pair magnetization and spatial correlations: longitudinal, transverse to detect phase transitions at a finite temperature [55,56]. In our study, we calculate the bipartite concurrence $\mathcal{C}(J_q, h)$ for the Heisenberg rung pair connected by exchange interaction $J_q=(J_q^z, J_q^{xy})$ in presence of the longitudinal field as

$$\mathcal{C}(J_q, h) = \max\left\{0, 4|c^T(J_q, h)| - 2\sqrt{\left[\frac{1}{4} + c^L(J_q, h)\right]^2 - [m'(J_q, h)]^2}\right\} \quad (12)$$

Where, $m'(J_q, h)$, $c^L(J_q, h)$ and $c^T(J_q, h)$ are the pair magnetization, the longitudinal and transverse component of bond order respectively, and these can be defined as:

$$m'(J_q, h) = \frac{1}{2}\langle S_{2j,1}^z + S_{2j,2}^z \rangle = -\frac{1}{2} \frac{\partial F_1(h, h', \beta)}{\partial h'} \quad (13)$$

$$c^L(J_q, h) = \langle S_{2j,1}^z S_{2j,2}^z \rangle = -\frac{1}{\beta} \frac{\partial [\ln Q_4(h, \beta)]}{\partial J_q^z} \quad (14)$$

$$c^T(J_q, h) = \langle S_{2j,1}^x S_{2j,2}^x \rangle = -\frac{1}{2\beta} \frac{\partial [\ln Q_4(h, \beta)]}{\partial J_q^{xy}} \quad (15)$$

Where, $F_1(h, h', \beta)$ is the free energy of one unit for which h, h' are the applied magnetic fields on the σ, S spins respectively. For the case, $h' = h$, $F(h, \beta) = F_1(h, h', \beta)$. For a better understanding of the spin arrangement of the σ spins within the unit, we calculate the longitudinal bond order $c^L(J_c, h)$ for the $\sigma - \sigma$ and $c^L(J_d, h)$ for the diagonal $\sigma - S$ spin pairs as:

$$c^L(J_c, h) = \langle \sigma_{2j+1,1} \sigma_{2j+1,2} \rangle = -\frac{1}{\beta} \frac{\partial [\ln Q_4(h, \beta)]}{\partial J_c} \quad (16)$$

$$c^L(J_d, h) = \langle \sigma_{2j+1,1} S_{2j+1,2}^z \rangle = -\frac{1}{4\beta} \frac{\partial [\ln Q_4(h, \beta)]}{\partial J_d} \quad (17)$$

However, the $c^L(J_q, h)$, $c^T(J_q, h)$, and the $\mathcal{C}(J_q, h)$ are shown in Fig.5. (a), (b) and (c) respectively for all four phases (i) the SRFM, (ii) the AAFM, (iii) the Dimer,

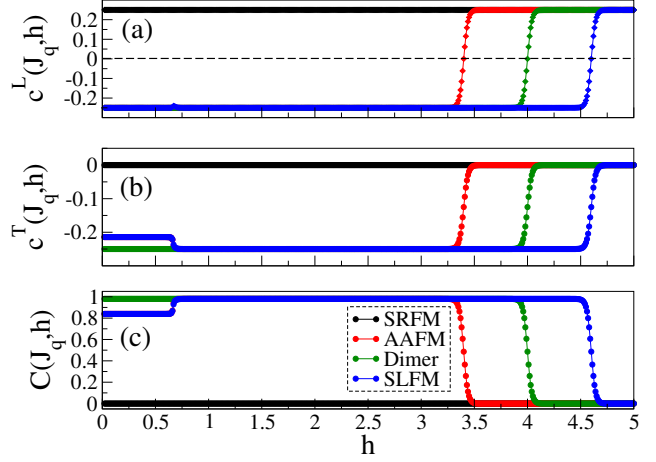


Figure 5. (a) Longitudinal bond order $c^L(J_q, h)$, (b) transverse bond order $c^T(J_q, h)$, (c) Quantum concurrence $\mathcal{C}(J_q, h)$ for the Heisenberg spin pair $S - S$ connected by rung strength J_q are shown as a function h . Black, red, green, and blue colors represent four phases: the SRFM ($J_q = 0.2, J_d = 2.0$), the AAFM ($J_q = 2.0, J_d = 0.4$), the Dimer ($J_q = 2.0, J_d = 1.0$), and the SLFM ($J_q = 2.0, J_d = 1.6$) respectively at $T/J_c = 0.02$.

and (iv) the SLFM. Fig.5 can be analyzed separately for different GS phases by approximating the partition function $Q_4(h, \beta)$ of Eq.3, as we mentioned earlier in Sec.4.1.1 that d_0, b_0 , and a_0 can describe the $m = 0, 1/4$, and $1/2$ plateau phases respectively for different limits of exchange parameters J_q, J_d , and field h .

The partition function for the SRFM phase having lower J_q and higher J_d can be written for three plateau phases: $m = 0, 1/4, 1/2$ as below-

$$Q_4(h, \beta) \approx \begin{cases} e^{-\frac{\beta}{4}(J_q^z + J_c - 4J_{cq} - 4J_d)} & m=0 \\ 4e^{-\frac{\beta}{4}(J_q^z - J_c - 4h)} & m=1/4 \\ e^{-\frac{\beta}{4}(J_q^z + J_c + 4J_{cq} + 4J_d - 8h)} & m=1/2 \end{cases} \quad (18)$$

In all of the plateaus, $c^L(J_q, h) = \frac{1}{4}$ and $c^T(J_q, h) = 0$ emphasizes the Ising dominance with the ferromagnetic alignment of the spins along the Heisenberg rung as shown in Fig.5.(a), and (b) respectively. The ferromagnetic alignment suggests $m'(J_q, h) = \pm 1/2$ and so the Eq.12 demands the $\mathcal{C}(J_q, h)$ to be always zero, which in other words can be thought of as there is no quantum concurrence or no quantum entanglement between the two S spins as shown in Fig.5. (c). It is to be noticed that $m'(J_q, h) = \pm 1/2$ represents the P-I phase as shown in Fig.3.b.(i). It can now be stated that the P-I phase is a pure state.

For the other three phases: the AAFM, the Dimer, and the SLFM with sufficiently larger J_q , the magnetization can be analyzed from the $Q_4(h, \beta)$ for various limits of the system parameter Δ_2 . We discuss the quantum concurrence for the plateau phases by writing down the partition functions separately.

(i) $m = 0$ plateau:

The partition function in this phase can be written as

$$Q_4(h, \beta) \approx 2e^{\frac{\beta(J_q^z + J_c)}{4}} \left[\text{Cosh}\left[\frac{\beta J_q^{xy}}{2}\right] + \text{Cosh}\left[\frac{\beta J_q^{xy} \Delta_2}{2}\right] \right] \quad (19)$$

The longitudinal bond order $c^L(J_q, h)$ in this case is $-1/4$ as shown in Fig.5.(a) whereas, the transverse bond order $c^T(J_q, h)$ is controlled by the interplay of the two terms in the partition function. For the Dimer phase ($\Delta_2 = 1$), the $c^T(J_q, h) = -1/4$, whereas, for the AAFM and SLFM phases ($\Delta_2 > 1$), $c^T(J_q, h)$ is less in magnitude as compared to the Dimer phase as shown in Fig.5. (b). The large transverse correlation along the Heisenberg spin pairs results in large $\mathcal{C}(J_q, h)$ close to unity for the AAFM and SLFM phases and it is maximum (unity) for the Dimer phase as shown in Fig.5.(c).

(ii) $m = 1/4$ plateau

The approximated partition function in this magnetic phase is

$$Q_4(h, \beta) \approx 2e^{\frac{\beta}{4}(J_q^z - J_c + 4h)} \text{Cosh}\left[\frac{\beta J_q^{xy}}{2}\right] \quad (20)$$

From the above partition function, one can obtain $c^L(J_c, h) = 1/4$, which implies the polarization of the σ spin pairs along the longitudinal field and it represents the P-II phase. In this plateau phase, the Heisenberg spin pairs have the longitudinal $c^L(J_q, h)$ and the transverse bond order $c^T(J_q, h)$ both as $-1/4$ and it is shown in Fig.5.(a), and (b). The maximum value of $c^T(J_q, h)$ in this phase results in giving the maximum concurrence $\mathcal{C}(J_q, h)$ equal to unity for all the phases: (i) the AAFM, (ii) the Dimer, and (iii) the SLFM as shown in Fig.5. (c). The Eq.20 has no J_d dependence implying the Ising and HB rungs are isolated. From these results, one can remark that the P-II is maximally entangled due to the strong singlet formation along the HB rung.

(iii) $m = 1/2$ plateau

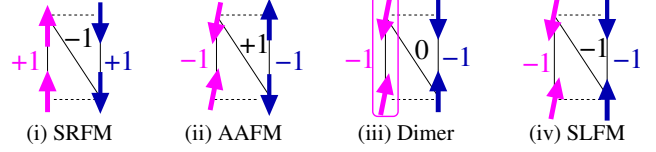
In this plateau phase, the partition function can be written as

$$Q_4(h, \beta) \approx e^{-\frac{\beta}{4}(J_q^z + J_c + 4J_{cq} + 4J_d - 8h)}, \quad (21)$$

which is exactly the same as discussed before for the SRFM phase. The exponent of the partition function suggests that all the longitudinal bond orders $c^L(J_q, h)$, $c^L(J_c, h)$, and $c^L(J_d, h)$ are $1/4$ and it is the signature of the FP phase with vanishing transverse bond order along the Heisenberg exchange J_q . The maximum longitudinal bond order and vanishing transverse bond order in the FP phase ensure that it is a pure state.

4.1.3. Quantum phase diagrams In this section, we analyze the quantum phases as a function of J_d and J_q at different longitudinal magnetic fields $h = 0, 1, 2$,

Ground-state phases :



Plateau phases :

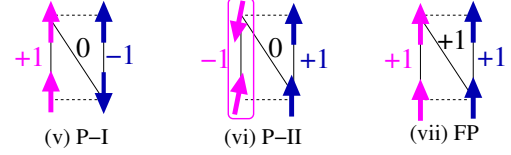


Figure 6. Schematics of the GS and the plateau phases are shown. Sign of the bond orders with exchange interactions J_q, J_d , and J_c are shown in magenta, black, and blue colors respectively. Boxes represent the perfect singlet Dimer formation.

Table 1. Quantum Phase Index (QPI) for different phases.

Phases	$Sign[c^L(J_q, h)]$	$Sign[c^L(J_d, h)]$	$Sign[c^L(J_c, h)]$	QPI
(i) SRFM	+1	-1	+1	2
(ii) AAFM	-1	+1	-1	-2
(iii) Dimer	-1	0	-1	-3
(iv) SLFM	-1	-1	-1	-4
(v) P-I	+1	0	-1	1
(vi) P-II	-1	0	+1	-1
(vii) FP	+1	+1	+1	4

and 3. For the sake of completeness, we show the $h = 0$ quantum phases (i.e., the zero field GS phases), which are studied earlier in [58]. To characterize the quantum phases uniquely, we define the quantum phase index (QPI) which is a function of three different bond orders within the unit cell of the lattice and can be written as

$$QPI = 2\text{Sign}[c^L(J_q, h)] + \text{Sign}[c^L(J_d, h)] + \text{Sign}[c^L(J_c, h)] \quad (22)$$

Where $\text{Sign}[x]$ is the signum function and can be defined as

$$\text{Sign}[x] = \begin{cases} 1 & \text{for } x > 0 \\ 0 & \text{for } x = 0 \\ -1 & \text{for } x < 0 \end{cases} \quad (23)$$

The spin arrangements and the signum values of the longitudinal bond orders along Heisenberg rung $c^L(J_q, h)$, diagonal spin pair $c^L(J_d, h)$, and Ising rung $c^L(J_c, h)$ are shown for the quantum phases in Fig.6. The signum value of the bond orders and the corresponding unique QPI for different quantum phases are tabulated in Table.1.

We analyze different plateau phases in the plane of $J_q - J_d$ for different values of h as shown in Fig.7.(i)-(iv). As it is seen in Fig.7.(i), $h = 0$ phase diagram represents four GS phases: (i) the SRFM, (ii) the

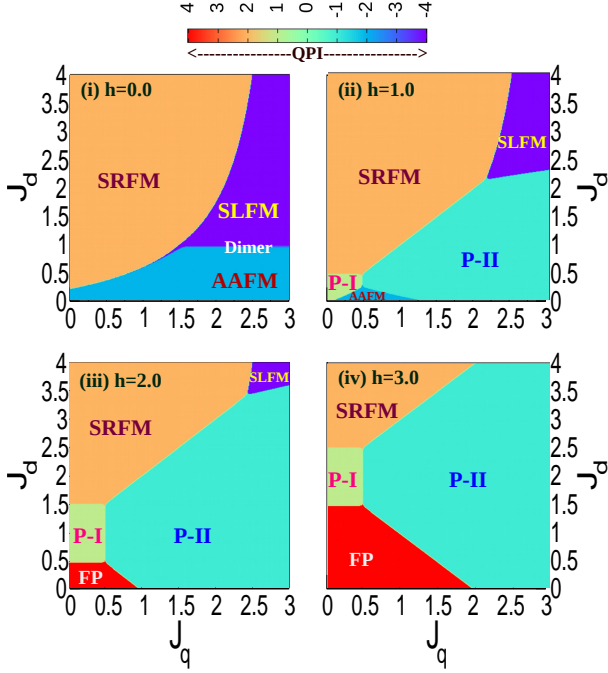


Figure 7. Quantum Phase Index (QPI) is shown for five longitudinal fields $h = 0, 1, 2, 3$ from (i)-(iv) in sequence. The color bar shows the QPI as defined in Eq.22. The QPI values 2, -2, -3, -4, 1, -1, 4 represent quantum phases: the SRFM, the AAFM, the Dimer, the SLFM, the P-I, the P-II, and the FP phases respectively.

AAFM, (iii) the Dimer, and (iv) the SLFM with the four distinct QPI values as 2, -2, -3, and -4 respectively. Fig. 7(ii) shows a few plateau phases along with the non-magnetic GS phases for the field $h = 1.0$. In this phase diagram, the P-I and P-II phases are shown with QPI numbers 1, and -1 respectively. With the low J_q value, the SRFM phase transit to P-I, whereas, in the vicinity of the SRFM-SLFM phase boundary, the regime with comparable J_q and J_d transit to P-II phase which is interesting and can be analyzed by writing down the critical fields for different limits of J_q . The spin gap or the critical field h_{c1} for the SRFM phase in different J_q limits can be obtained as

$$h_{c1} \approx \begin{cases} (J_d + 1/2) & \text{for } J_q < J_c \\ (1 + J_d - \frac{J_q^z}{2} - \frac{J_q^{xy}}{2}) & \text{for } J_q > J_c \end{cases} \quad (24)$$

From the above equation, by considering $h_{c1} = 1$, the phase boundaries between the SRFM-P-I and the SRFM-P-II phases can be obtained as $J_d = 0.5$ and $J_d \approx J_q$ respectively and these boundaries are noticed in Fig.7. (ii).

Similarly, the spin gap h_{c1} for the AAFM, the Dimer, and the SLFM phases can be written as a

function of J_q and Δ in the following manner

$$h_{c1} \approx \frac{1}{2} + \frac{1}{\beta} \ln \left[1 + \frac{\text{Cosh} \left[\frac{\beta J_q^{xy} \Delta_2}{2} \right]}{\text{Cosh} \left[\frac{\beta J_q^z}{2} \right]} \right] \quad (25)$$

The critical fields h_{c1} in Fig.2. (ii)-(iv) for the AAFM (0.7), the Dimer (0.5), and the SLFM (0.7) phases agree well with the above equation. Also, from the Eq.25, one can determine the phase boundaries between the AAFM-P-II, and the SLFM-P-II as a function of system parameters J_q , J_d or Δ_2 . However, the major part of the parameter space in Fig.7. (iii) is occupied by P-II due to the low spin gap in the AAFM, the Dimer, and the SLFM phases. In Fig. 7(iii), the P-II occupies the largest area and replaces the AAFM phase completely for the field $h = 2$. A small area of the FP phase emerges in this case for very small values of J_q and J_d in Fig.7.(iii).

The FP phase appears either from the P-I or P-II phase on the application of the critical field h_{c2} . This critical field can be written as a function of the system parameters in the following way

$$h_{c2} \approx \begin{cases} (J_d + 3/2) & \text{for P-I phase} \\ \frac{(J_q^z + 2J_d + 2)}{2} & \text{for P-II phase} \end{cases} \quad (26)$$

From the above equation, by taking $h_{c2} = 2$, one can determine the phase boundary between the P-I-FP phase as $J_d = 1/2$. Similarly, the P-II-FP phase boundary can also be obtained from the above equation. For $h = 3$ in 7. (iv), the SLFM phase is replaced by P-II, whereas, for the large J_d value, the SRFM phase still exists in the magnetic phase diagram due to the largest spin gap $h_{c2} = (J_d + 3/2)$ as in Eq.26. With an even larger field value, all other phases vanish and the FP phase occupies the phase diagram completely.

4.2. Magnetization process in the presence of a transverse field

Using many experimental techniques in general, this kind of system is synthesized in powder form or single crystal form and so to understand the directional dependence of the field on the magnetization, we study the effect of the transverse field h^x in our model [2,3]. In the presence of h^x , the Hamiltonian of different units do not commute to each other, and therefore, the TM method never works, we use the ED method to show the finite size scaling of magnetization for three system sizes and then analyze the spin density for $N = 24$.

4.2.1. Transverse component of magnetization It is to be mentioned that all four GS phases are in the $S^z = 0$ sector, and so it does not change the longitudinal but rather the transverse component of magnetization on

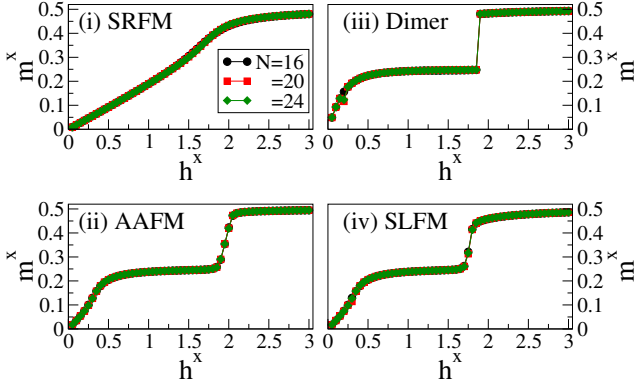


Figure 8. Transverse magnetization m^x is shown as a function of the transverse field h^x for four phases: (i) SRFM ($J_q = 0.2$, $J_d = 2.0$), (ii) AAFM ($J_q = 2.0$, $J_d = 0.4$) (iii) Dimer ($J_q = 2.0$, $J_d = 1.0$), and (iv) SLFM ($J_q = 2.0$, $J_d = 1.6$). Black, red, and green colors represent the system sizes $N = 16, 20$, and 24 respectively.

the application of an external transverse field h^x . We calculate the transverse magnetization m^x in terms of spin density $\langle S_i^x \rangle$ at each site i as-

$$m^x = \frac{1}{N} \sum_{i=1}^N \langle S_i^x \rangle \quad (27)$$

In Fig.8[(i)-(iv)], we show the transverse (along $+x$ direction) magnetization for all four phases: (i) the SRFM, (ii) the AAFM, (iii) the Dimer, and (iv) the SLFM with the corresponding set of chosen J_q , J_d values as in section 4.1.1 for the system sizes $N = 16, 20$, and 24 . In the SRFM phase, the m^x shows continuous variation with the field h^x up to saturation value. In this phase, the GS has Ising bond dominance for all the spins, and therefore the spins along the x-direction get smoothly oriented along the field. In the AAFM phase, the curve increases smoothly and then it shows a $m^x \approx 1/4$ plateau-like behavior in the range $0.45 < h^x < 1.75$, and afterward it jumps to full saturation. A similar behavior is noticed in the Dimer phase as well in which the plateau onsets at a field $h^x = 0.4$. In this case, the jump from the $m^x = 1/4$ plateau to saturation is much faster than in the case of the AAFM phase. In the SLFM phase for $h^x < 0.7$, m^x increases smoothly, and then it forms the plateau-like structure for $0.7 < h^x < 1.7$. It shows a sudden jump almost around $h^x = 1.75$ and slowly reaches saturation magnetization for higher h^x . From all the subfigures, it is noticed that there is a negligibly small finite-size effect. In the next subsection, we analyze the $m^x = 1/4$ plateau mechanism for all the phases based on the spin density.

4.2.2. Transverse component of spin density For a more detailed understanding, we show the color map of the spin density $\langle S_i^x \rangle$ in all four phases for $N = 24$. It is

to be mentioned that the $\sigma - \sigma$ and $S - S$ pairs alternate with site index i . To be more specific, $\sigma - \sigma$ pairs take the site indices $[1, 2, 5, 6, \dots]$ whereas, $S - S$ pairs take the indices $[3, 4, 7, 8, \dots]$ as shown in all subfigures of Fig.9. In Fig.9.(i), $\langle S_i^x \rangle$ varies continuously as h^x increases for all the sites. As the GS of the SRFM has only Ising interactions dominance and there is no transverse spin correlation, all the spins continuously get oriented along h^x in this phase. In the AAFM phase, the $S - S$ pair has a strong transverse spin correlation whereas, the $\sigma - \sigma$ rung pairs are weak and are equations continuously with an increase in h^x as shown in the color map Fig.9. (ii). Saturation is attained by an even further increase of field when it breaks the strong $S - S$ pair at $h^x = 1.75$. As shown in Fig.9. (iii) for the Dimer phase, the continuous increase of m^x is similar to the AAFM phase but a sudden jump at $h^x = 1.7$ is noticed because of unbinding of the perfect $S - S$ singlet pairs. Fig.9.(iv) shows $\langle S_i^x \rangle$ for the SLFM phase. As in the GS of this phase, both the Ising pairs and Heisenberg pairs are aligned parallel but spins of opposite legs are aligned oppositely, with the increase in h^x , it is noticed that all the Ising dimer pairs are continuously broken until the magnetization reaches to $1/4$. An even further increase in h^x does not easily close the spin gap and results in a large $m^x = 1/4$ plateau until a field $h^x = 1.75$ is applied to break the Heisenberg rung $S - S$ pairs.

5. Summary

In this paper, we study the effect of external magnetic field on the GS phases of Hamiltonian in Eq.1 of a frustrated spin- $\frac{1}{2}$ two-leg ladder with alternate Ising and Heisenberg type of rung and Ising type of interaction in the leg and diagonal. This model has a few similarities to one of the earlier studied models where leg and diagonal exchanges are Ising type but all the rung exchanges are Heisenberg type in which on applying the magnetic field, a magnetic phase SB appears [52]. In our model, alternate rungs are Ising-Heisenberg type due to which the zero field GS phases and the plateau phases depend upon the competing Ising and Heisenberg rung exchanges as well. Tuning of the exchange parameters in the model Hamiltonian can give rise to four GS phases: (i) the SRFM, (ii) the AAFM, (iii) the Dimer, and (iv) the SLFM, whose spin arrangements are schematically represented in Fig.1.b. [(i)-(iv)]. We analyzed the magnetization behavior in the presence of external magnetic fields: longitudinal and transverse.

In the presence of the longitudinal magnetic field h , the GS shows three magnetic plateaus: the first one is due to the finite spin gap, the second plateau at $m = 1/4$ is formed due to the polarization of either

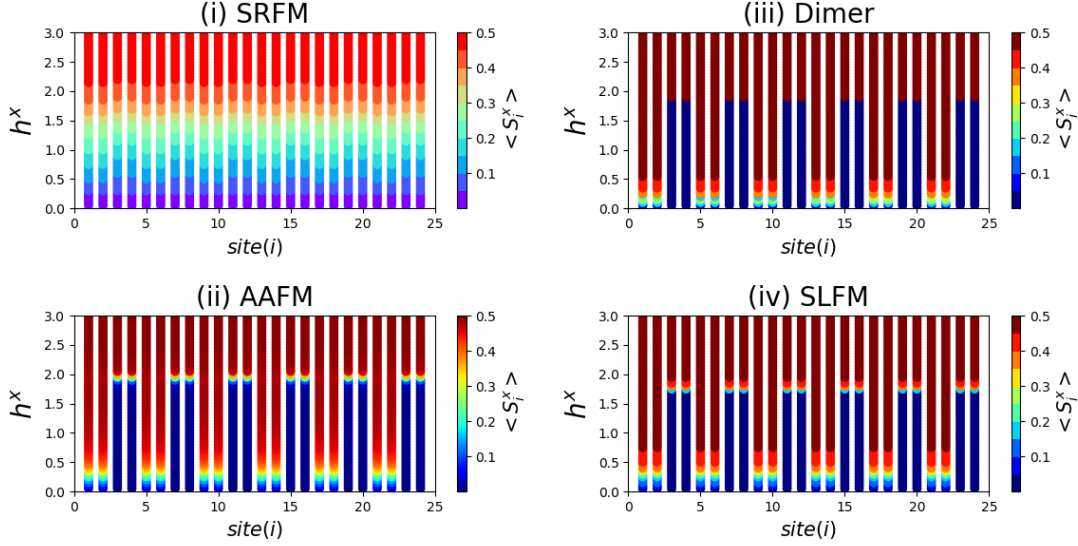


Figure 9. Transverse component of spin density $\langle S_i^x \rangle$ at each site i for four phases: (i) SRFM ($J_q = 0.2$, $J_d = 2.0$), (ii) AAFM ($J_q = 2.0$, $J_d = 0.4$) (iii) Dimer ($J_q = 2.0$, $J_d = 1.0$), and (iv) SLFM ($J_q = 2.0$, $J_d = 1.6$) are shown for system size $N = 24$. Along the horizontal axis, the site index i for each spin is shown. Along the vertical axis, the transverse field h^x is varied. The color bar shown in all subfigures represents the amplitude of $\langle S_i^x \rangle$ and it varies from 0 to 0.5 for spin-1/2 systems.

Ising or Heisenberg type of rung spin dimers along the field. This can be of two types as shown in Fig.3.b. In the SRFM phase, the Heisenberg rung spin pairs $S - S$ are polarized giving rise to “ $m = 1/4$ plateau type-1” or “P-I” phase as shown in Fig.3.b.(i). But for the other three zero field GS phases: the AAFM, the Dimer, and the SLFM, the $\sigma - \sigma$ spins are polarized at $m = 1/4$ and give rise to “ $m = 1/4$ plateau type-2” or “P-II” phase as shown in Fig.3.b.(ii). In the presence of a large external field in all phases, all of the spins are completely polarized along the field and form the third plateau at the saturation magnetization $m = 1/2$ which is named FP. The $m = 1/4$ plateau width is sensitive to the parameter values as obtained in Eq.7. We also notice that two plateaus are connected by jumps in the magnetization curve and this is because of the unpairing of either all $S - S$ (for P-I) or all $\sigma - \sigma$ (for P-II) rung dimers.

To understand the quantum nature of the wave function of the GS, we calculate the quantum fidelity and quantum concurrence in the presence of a longitudinal field. In all four phases, fidelity shows deviation from unity at the critical fields of magnetic phase transitions as shown in Fig.4. We note that the discontinuities in fidelity represent the overlap of the plateau phases. The quantum concurrence shown in Fig.5.c measures the entanglement between two spins at the Heisenberg rung. The concurrence is always zero as a function of the field for the SRFM phase, and it means that the SRFM phase is a pure state. Whereas, in other phases: the AAFM, the Dimer, and

the SLFM, the concurrence has a finite value both at $m = 0$. In the $m = 0$ plateau phase, the concurrence is a function of the exchange interactions for the AAFM, and the SLFM phases and it is maximum for the Dimer phase. The concurrence is zero for the P-I phase and FP phase. Whereas it is maximum for the P-II phase as it forms the isolated singlet Dimers along the Heisenberg rung. So, one can state that the P-II phase is maximally entangled, whereas, P-I and FP phases are the pure states. However, all of the jumps in the magnetization can be indirectly predicted based on the jumps in concurrence as shown in Fig.5.c.

We define QPI to uniquely identify the quantum phases in the exchange parameter J_q - J_d plane for a finite longitudinal field h . The unique QPI values for different quantum phases are tabulated in Table.1. The effect of the longitudinal magnetic field on the GS phases is shown in Fig.7.[(i)-(iv)]. For a sufficiently larger longitudinal field $h = 1.0$, the Dimer phase disappears, and two types of $m = 1/4$ plateaus: P-I, P-II appear. At a very large field $h = 3.0$, it is noticed that the P-I, P-II, and FP phases dominate in the phase diagram. The phase boundaries among the quantum phases can easily be obtained from the analytical expression of the critical fields of phase transitions.

In the SRFM phase, spin alignments are along the z direction and there is weak exchange interaction along the $+x$ direction in the Heisenberg rung dimers, therefore, magnetization m^x shows a continuous variation till saturation on the application of a

transverse field. In other phases: the AAFM, the Dimer, and the SLFM, the magnetization process can be understood in terms of two sublattice behaviors. The sublattice with $\sigma - \sigma$ dimer is paramagnetic along x, whereas, in the other sublattice, the Heisenberg spin pair $S - S$ dimer has a strong transverse exchange component which induces a finite spin gap in the system. As a consequence, at a lower value of the transverse field, the system shows a continuous behavior in the magnetization curve due to gradual change of m^x of $\sigma - \sigma$ spins up to $m^x = 1/4$ with an increase in h^x as shown using spin density in Fig.9. [(ii)-(iv)]. With further increase in field, at a critical value, the magnetization curve shows a sudden jump from $m^x \approx 1/4$ to $1/2$ for the three phases: the AAFM, the Dimer, and the SLFM, and this phase transition seems to be of the first order. The plateau width is sensitive to the set of parameters or the set of exchange interactions J_q and J_d in the presence of a transverse

field also.

In conclusion, this model system is unique because of the alternate Ising-Heisenberg rung exchange and gives many insightful mechanisms of the plateau and jumps both in the presence of longitudinal and transverse fields. The magnetic properties of such systems can be utilized in designing quantum switches, magnetic memories, and other similar devices. Also, these systems might have tremendous applications in quantum information processing and quantum computation because of the entangled states.

6. Acknowledgements

M.K. thanks SERB Grant Sanction No. CRG/2020/000754 for the computational facility. S.S.R. thanks CSIR-UGC for financial support.

7. Appendix 1

The partition function in presence of a longitudinal field h for N sites, $Q_N(h, \beta)$ with Hamiltonian H can be written as-

$$Q_N(h, \beta) = \text{Tr} \left(e^{-\beta \mathbf{H}} \right) \quad (28)$$

Where, Tr means trace of the matrix, $\beta = 1/(k_B T)$ and k_B is the Boltzmann constant. Using explicit configuration basis for the system, Eq. 28 is rewritten in the following form,

$$Q_N(h, \beta) = \sum_{\{\sigma, S\}} \langle \cdots, \sigma_{2j-1,1}, \sigma_{2j-1,2}, S_{2j,1}, S_{2j,2}, \cdots | e^{-\beta \mathbf{H}} | \cdots, \sigma_{2j-1,1}, \sigma_{2j-1,2}, S_{2j,1}, S_{2j,2}, \cdots \rangle .$$

Here the summation is over all possible configurations $\{\sigma, S\}$ of the system. For a given configuration, $|\cdots, \sigma_{2j-1,1}, \sigma_{2j-1,2}, S_{2j,1}, S_{2j,2}, \cdots \rangle$ represents a basis state. In our case, the system is composed of $n = N/4$ units, and for each unit, the Hamiltonian is written in Eq.1. The partition function of the entire ladder can be written as:

$$Q_N(h, \beta) = \sum_{\sigma} \langle \cdots, \sigma_{2j-1,1}, \sigma_{2j-1,2}, \cdots | \prod_{j=1}^n \mathbf{T}_j | \cdots, \sigma_{2j-1,1}, \sigma_{2j-1,2}, \cdots \rangle$$

where $T_i = \sum_{\{S\}_i} \langle S_{2i,1}, S_{2i,2} | e^{-\beta \mathbf{H}_i(\sigma, S)} | S_{2i,1}, S_{2i,2} \rangle$ is well-known transfer matrix operator for each unit. Here the summation is over $\{S\}_i$ which represents all possible configurations of spins $S_{2i,1}$ and $S_{2i,2}$ (from the i^{th} unit). It may be noted that T_i does not contain the components of spin S operators and it has only σ variables, namely, $\sigma_{2i-1,1}, \sigma_{2i-1,2}, \sigma_{2i+1,1}$ and $\sigma_{2i+1,2}$. Since, the Hamiltonians of each unit commute to each other, introducing identity operators $I = \sum_{\{\sigma\}_i} |\sigma_{2i-1,1}, \sigma_{2i-1,2} \rangle \langle \sigma_{2i-1,1}, \sigma_{2i-1,2}|$ between successive \mathbf{T} operators, we can finally write the partition function as the trace of the n -th power of a small (4×4) transfer matrix \mathbf{P} . We have $Q_N(h, \beta) = \text{Tr}(\mathbf{P}^n)$. The elements of the transfer matrix are given by

$$P_{(\sigma_{2i-1,1}, \sigma_{2i-1,2}), (\sigma_{2i+1,1}, \sigma_{2i+1,2})} = \langle \sigma_{2i-1,1}, \sigma_{2i-1,2} | \mathbf{T}_i | \sigma_{2i+1,1}, \sigma_{2i+1,2} \rangle \quad (29)$$

Before we construct and diagonalize the \mathbf{P} matrix, we first need to carry out the trace over the configurations $\{S\}_i$ to find out the form of \mathbf{T}_i . Since $\mathbf{T}_i = \sum_{\{S\}_i} \langle S_{2i,1}, S_{2i,2} | e^{-\beta \mathbf{H}_i(\sigma, S)} | S_{2i,1}, S_{2i,2} \rangle$, if we take the eigenstate basis of \mathbf{H}_i , we will get \mathbf{T}_i as the summation over exponential of eigenvalues of $-\beta \mathbf{H}_i$. Next, we calculate the eigenvalues of \mathbf{H}_i operator. Now, y considering,

$$\begin{aligned} a &= J_d (\sigma_{2j-1,2}^z + \sigma_{2j+1,2}^z) + J_{cq} (\sigma_{2j-1,1}^z + \sigma_{2j+1,1}^z) + h \\ b &= J_d (\sigma_{2j-1,1}^z + \sigma_{2j+1,1}^z) + J_{cq} (\sigma_{2j-1,2}^z + \sigma_{2j+1,2}^z) + h \\ c &= \frac{J_c}{2} (\sigma_{2j-1,1}^z \sigma_{2j-1,2}^z + \sigma_{2j+1,1}^z \sigma_{2j+1,2}^z) \end{aligned}$$

$$d = \frac{h}{2} (\sigma_{2j-1,1}^z + \sigma_{2j-1,2}^z + \sigma_{2j+1,1}^z + \sigma_{2j+1,2}^z),$$

$$f = c + d$$

Hamiltonian (Eq. 1) for the j^{th} geometrical unit can be written as-

$$\mathbf{H}_j = \frac{J_q^{xy}}{2} (S_{2j,1}^+ S_{2j,2}^- + S_{2j,1}^- S_{2j,2}^+) + J_q^z (S_{2j,1}^z S_{2j,2}^z) + a S_{2j,1}^z + b S_{2j,2}^z + f$$

We can write down the following Hamiltonian matrix in the eigenstate basis of $S_{2j,1}^z S_{2j,2}^z$ operator as

$$H_j = \begin{bmatrix} \frac{J_q^z}{4} + \frac{(a+b)}{2} + f & 0 & 0 & 0 \\ 0 & -\frac{J_q^z}{4} + \frac{(a-b)}{2} + f & \frac{J_q^{xy}}{2} & 0 \\ 0 & \frac{J_q^{xy}}{2} & -\frac{J_q^z}{4} - \frac{(a-b)}{2} + f & 0 \\ 0 & 0 & 0 & \frac{J_q^z}{4} - \frac{(a+b)}{2} + f \end{bmatrix}$$

The Hamiltonian matrix comes up with its four eigenvalues from three S_{SS}^z sectors based on S-S pairs-

(i) From $S_{SS}^z = 1$ sector (formed by S-S pair)

$$\theta_1 = (f + \frac{J_q^z}{4}) + \frac{(a+b)}{2}$$

(ii) From $S_{SS}^z = -1$ sector (formed by S-S pair)

$$\theta_2 = (f + \frac{J_q^z}{4}) - \frac{(a+b)}{2}$$

(iii) From $S_{SS}^z = 0$ sector (formed by S-S pair)

$$\theta_3 = (f - \frac{J_q^z}{4}) + \frac{\sqrt{(J_q^{xy})^2 + (a-b)^2}}{2}$$

$$\theta_4 = (f - \frac{J_q^z}{4}) - \frac{\sqrt{(J_q^{xy})^2 + (a-b)^2}}{2}$$

We note that the eigenvalues ($\theta_{k'}$) are functions of σ variables, namely $\sigma_{2j-1,1}$, $\sigma_{2j-1,2}$, $\sigma_{2j+1,1}$ and $\sigma_{2j+1,2}$. Using these eigenvalues, we rewrite \mathbf{T}_j as,

$$\mathbf{T}_j = \sum_{\{S\}_j} \langle S_{2j,1}, S_{2j,2} | e^{-\beta \mathbf{H}_j(\sigma, S)} | S_{2j,1}, S_{2j,2} \rangle$$

$$= \sum_{k'=1}^4 e^{-\beta \theta_{k'}}.$$

$$= 2e^{-\beta f} \left[e^{-\frac{\beta J_q^z}{4}} \text{Cosh}\left(\frac{\beta(a+b)}{2}\right) + e^{\frac{\beta J_q^z}{4}} \text{Cosh}\left(\frac{\beta J_q^{xy}}{2} \sqrt{1 + \frac{(a-b)^2}{(J_q^{xy})^2}}\right) \right]$$

$$\text{Further, we consider- } e^{\frac{\beta J_q^z}{4}} = Q, \quad e^{\frac{\beta J_c}{4}} = C,$$

$$e^{\frac{\beta h}{4}} = H, \quad \frac{(J_{cq} + J_d)}{2} = X, \quad \frac{(J_{cq} - J_d)^2}{(J_q^{xy})^2} = Y,$$

$$\text{and also, } \Delta_1 = \sqrt{1+Y}, \quad \Delta_2 = \sqrt{1+4Y}.$$

The Transfer matrix for one unit becomes -

$$\mathbf{P} = \begin{bmatrix} p & q & q & r \\ q & s & u & v \\ q & u & s & v \\ r & v & v & w \end{bmatrix}.$$

Where,

$$p = 2e^{-\beta(J_c/4+h)}$$

$$\times \left[Q^{-1} \text{Cosh}(\beta(2X+h)) + Q \text{Cosh}\left(\frac{\beta J_q^{xy}}{2}\right) \right]$$

$$q = 2e^{-\beta(h/2)}$$

$$\times \left[Q^{-1} \text{Cosh}(\beta(X+h)) + Q \text{Cosh}\left(\frac{\beta J_q^{xy} \Delta_1}{2}\right) \right]$$

$$r = 2e^{-\beta(J_c/4)}$$

$$\times \left[Q^{-1} \text{Cosh}(\beta h) + Q \text{Cosh}\left(\frac{\beta J_q^{xy}}{2}\right) \right]$$

$$s = 2e^{\beta(J_c/4)}$$

$$\times \left[Q^{-1} \text{Cosh}(\beta h) + Q \text{Cosh}\left(\frac{\beta J_q^{xy} \Delta_2}{2}\right) \right]$$

$$u = 2e^{\beta(J_c/4)}$$

$$\times \left[Q^{-1} \text{Cosh}(\beta h) + Q \text{Cosh}\left(\frac{\beta J_q^{xy}}{2}\right) \right]$$

$$v = 2e^{\beta(h/2)}$$

$$\times \left[Q^{-1} \text{Cosh}(\beta(-X+h)) + Q \text{Cosh}\left(\frac{\beta J_q^{xy} \Delta_1}{2}\right) \right]$$

$$w = 2e^{-\beta(J_c/4-h)}$$

$$\times \left[Q^{-1} \text{Cosh}(\beta(-2X+h)) + Q \text{Cosh}\left(\frac{\beta J_q^{xy}}{2}\right) \right]$$

From $|P - \lambda I_4| = 0$, we get the eigenvalues in the form of

$$\lambda_4 = (s - u)$$

$$\lambda^3 - B_0 \lambda^2 - C_0 \lambda + D_0 = 0 \quad (30)$$

Here, λ_4 is one of the eigenvalues, whereas, the other three come from Eq.30. The coefficients of the equation are defined as:

$$B_0 = (s + u + w)$$

$$C_0 = [2(q^2 + v^2 - \frac{r^2}{2}) - pw + (p-w)(s+u)]$$

$$D_0 = [4qrv - 2pv^2 - 2q^2w + pw^2 - (s+u)(r^2 + pw)]$$

For the polynomial equation 30, the eigenvalues λ_i satisfy the relations-

$$\sum_{i=1}^3 \lambda_i = B_0, \quad \sum_{i=1}^3 \lambda_i \lambda_{i+1} = -C_0 \quad (31)$$

Now, let us make a very reasonable assumption to make the calculation easy. We assume, $\lambda_1 \gg \lambda_2 \gg \lambda_3$ are in descending order and λ_3 has the least contribution in the partition function so that Eq.31 can approximately be written as:

$$\lambda_1 + \lambda_2 = B_0, \lambda_1 \lambda_2 = -C_0 \quad (32)$$

The Eq. 32 leads us to getting other two eigenvalues:

$$\lambda_{1,2}^2 - B_0 \lambda_{1,2} - C_0 = 0$$

$$\Rightarrow \lambda_{1,2} = \frac{B_0 \pm \sqrt{B_0^2 + 4C_0}}{2} \quad (33)$$

We find Eq. 33 becomes much more simpler with further approximation in $\beta \rightarrow \infty$ limit as-

$$\begin{aligned} \lambda_1 &= (w + s + u) \\ &= 2e^{-\frac{\beta(J_c - 4h)}{4}} \left[Q^{-1} \text{Cosh}[\beta(h - 2X)] + Q \text{Cosh}\left[\frac{\beta J_q^{xy}}{2}\right] \right] \\ &+ \left[2Q^{-1} \text{Cosh}[\beta h] + Q \text{Cosh}\left[\frac{\beta J_q^{xy}}{2}\right] + Q \text{Cosh}\left[\frac{\beta J_q^{xy} \Delta_2}{2}\right] \right] \\ &\times 2e^{\frac{\beta(J_c)}{4}} \end{aligned} \quad (34)$$

$Q_N(h, \beta)$ takes the form as

$$\begin{aligned} Q_N(h, \beta) &= [\lambda_1^n + \lambda_2^n + \lambda_3^n + \lambda_4^n] \\ \rightarrow Q_N(h, \beta) &= \lambda_1^n \left[1 + \frac{\lambda_2^n}{\lambda_1^n} + \frac{\lambda_3^n}{\lambda_1^n} + \frac{\lambda_4^n}{\lambda_1^n} \right] \end{aligned}$$

For $n \rightarrow \infty$, and λ_1 being the largest, the partition function for the entire system and one unit become $Q_N(h, \beta) \approx \lambda_1^n$ and $Q_4(h, \beta) \approx \lambda_1$ respectively.

References

- [1] Nakamura T and Okamoto K 1998 *Physical Review B* **58** 2411
- [2] Guo S, Zhong R, Górnicka K, Klimczuk T and Cava R J 2020 *Chemistry of Materials* **32** 10670–10677
- [3] Kakarla D C, Yang Z, Wu H, Kuo T, Tiwari A, Li W H, Lee C, Wang Y Y, Lin J Y, Chang C et al. 2021 *Materials Advances* **2** 7939–7948
- [4] Dagotto E and Rice T M 1996 *Science* **271** 618–623 ISSN 0036-8075 URL <https://science.sciencemag.org/content/271/5249/618>
- [5] Chubukov A V 1991 *Phys. Rev. B* **44**(9) 4693–4696 URL <https://link.aps.org/doi/10.1103/PhysRevB.44.4693>
- [6] Chubukov A V, Sachdev S and Ye J 1994 *Physical Review B* **49** 11919
- [7] Hutchings M T Ikeda H M J M 1979 *Journal of Physics C, Solid State Physics* **18**(12) L739–L744
- [8] Park S, Choi Y J, Zhang C L and Cheong S W 2007 *Phys. Rev. Lett.* **98**(5) 057601 URL <https://link.aps.org/doi/10.1103/PhysRevLett.98.057601>
- [9] Mourigal M, Enderle M, Fåk B, Kremer R K, Law J M, Schneidewind A, Hiess A and Prokofiev A 2012 *Phys. Rev. Lett.* **109**(2) 027203 URL <https://link.aps.org/doi/10.1103/PhysRevLett.109.027203>
- [10] Drechsler S L, Volkova O, Vasiliev A N, Tristan N, Richter J, Schmitt M, Rosner H, Málek J, Klingeler R, Zvyagin A A and Büchner B 2007 *Phys. Rev. Lett.* **98**(7) 077202 URL <https://link.aps.org/doi/10.1103/PhysRevLett.98.077202>
- [11] Dutton S E, Kumar M, Soos Z G, Broholm C L and Cava R J 2012 *Journal of Physics: Condensed Matter* **24** 166001 URL <https://doi.org/10.1088/0953-8984/24/16/166001>
- [12] Dutton S E, Kumar M, Mourigal M, Soos Z G, Wen J J, Broholm C L, Andersen N H, Huang Q, Zbiri M, Toft-Petersen R and Cava R J 2012 *Phys. Rev. Lett.* **108**(18) 187206 URL <https://link.aps.org/doi/10.1103/PhysRevLett.108.187206>
- [13] Maeshima N, Hagiwara M, Narumi Y, Kindo K, Kobayashi T C and Okunishi K 2003 *Journal of Physics: Condensed Matter* **15** 3607–3618 URL <https://doi.org/10.1088/0953-8984/15/21/309>
- [14] Sandvik A W, Dagotto E and Scalapino D J 1996 *Phys. Rev. B* **53**(6) R2934–R2937 URL <https://link.aps.org/doi/10.1103/PhysRevB.53.R2934>
- [15] Johnston D C, Johnson J W, Goshorn D P and Jacobson A J 1987 *Phys. Rev. B* **35**(1) 219–222 URL <https://link.aps.org/doi/10.1103/PhysRevB.35.219>
- [16] Vekua T, Japaridze G and Mikeska H J 2003 *Physical Review B* **67** 064419
- [17] Richter J, Schulenberg J and Honecher A 2004 Quantum magnetism in two dimensions: From semi-classical néel order to magnetic disorder in quantum magnetism, ed. u. schollwöck, j. richter, djf farnell and rf bishop
- [18] Ogino T, Kaneko R, Morita S, Furukawa S and Kawashima N 2021 *Physical Review B* **103** 085117
- [19] Ogino T, Kaneko R, Morita S and Furukawa S 2022 *Physical Review B* **106** 155106
- [20] Luttinger J 1963 *Journal of mathematical physics* **4** 1154–1162
- [21] Sakai T, Nakanishi R, Yamada T, Furuchi R, Nakano H, Kaneyasu H, Okamoto K and Tonegawa T 2022 *Physical Review B* **106** 064433
- [22] Maiti D and Kumar M 2019 *Phys. Rev. B* **100**(24) 245118 URL <https://link.aps.org/doi/10.1103/PhysRevB.100.245118>
- [23] Balents L 2010 *Nature* **464** 199–208
- [24] Liao H J, Xie Z Y, Chen J, Liu Z Y, Xie H D, Huang R Z, Normand B and Xiang T 2017 *Physical review letters* **118** 137202
- [25] Bethe H 1931 *Zeitschrift für Physik* **71** 205–226
- [26] Barnes T, Dagotto E, Riera J and Swanson E 1993 *Physical Review B* **47** 3196
- [27] Johnston D, McQueeney R, Lake B, Honecker A, Zhitomirsky M, Nath R, Furukawa Y, Antropov V and Singh Y 2011 *Physical Review B* **84** 094445
- [28] Kumar M, Parvej A and Soos Z G 2015 *Journal of Physics: Condensed Matter* **27** 316001 URL <https://doi.org/10.1088/0953-8984/27/31/316001>
- [29] Chitra R, Pati S, Krishnamurthy H R, Sen D and Ramasesha S 1995 *Phys. Rev. B* **52**(9) 6581–6587 URL <https://link.aps.org/doi/10.1103/PhysRevB.52.6581>
- [30] White S R and Affleck I 1996 *Phys. Rev. B* **54**(14) 9862–9869 URL <https://link.aps.org/doi/10.1103/PhysRevB.54.9862>
- [31] Rahaman S S, Haldar S and Kumar M 2023 *Journal of Physics: Condensed Matter*
- [32] Rakov M V, Weyrauch M and Braiorr-Orrs B 2016 *Phys. Rev. B* **93**(5) 054417 URL <https://link.aps.org/doi/10.1103/PhysRevB.93.054417>
- [33] Mikeska H J and Kolezhuk A K 2004 *Quantum magnetism* 1–83
- [34] Wessel S, Normand B, Mila F and Honecker A 2017 *SciPost Physics* **3** 005
- [35] Morita S, Kaneko R and Imada M 2015 *Journal of the Physical Society of Japan* **84** 024720
- [36] Hijii K, Kitazawa A and Nomura K 2005 *Physical Review B* **72** 014449
- [37] Liu W Y, Gong S S, Li Y B, Poilblanc D, Chen W Q and Gu Z C 2022 *Science bulletin* **67** 1034–1041
- [38] Li S H, Shi Q Q, Batchelor M T and Zhou H Q 2017 *New Journal of Physics* **19** 113027
- [39] Agrapidis C E, van den Brink J and Nishimoto S 2019 *Phys.*

- Rev. B* **99**(22) 224418 URL <https://link.aps.org/doi/10.1103/PhysRevB.99.224418>
- [40] Ivanov N 2009 *arXiv preprint arXiv:0909.2182*
- [41] Sakai T and Yamamoto S 1999 *Physical Review B* **60** 4053
- [42] Sakai T and Okazaki N 2000 *Journal of Applied Physics* **87** 5893–5895
- [43] Naseri M S and Mahdavifar S 2017 *Physica A: Statistical Mechanics and its Applications* **474** 107–114
- [44] Zad H A and Ananikian N 2018 *Journal of Physics: Condensed Matter* **30** 165403
- [45] Japaridze G I and Pogosyan E 2006 *Journal of Physics: Condensed Matter* **18** 9297
- [46] Moradmard H, Shahri Naseri M and Mahdavifar S 2014 *Journal of Superconductivity and Novel Magnetism* **27** 1265–1271
- [47] Dey D, Das S, Kumar M and Ramasesha S 2020 *Physical Review B* **101** 195110
- [48] Oshikawa M, Yamanaka M and Affleck I 1997 *Phys. Rev. Lett.* **78**(10) 1984–1987 URL <https://link.aps.org/doi/10.1103/PhysRevLett.78.1984>
- [49] Strečka J and Jascur M 2003 *Journal of Physics: Condensed Matter* **15** 4519
- [50] Verkholyak and Strečka 2013 *Condensed Matter Physics* **16** 13601 ISSN 1607-324X URL <http://dx.doi.org/10.5488/CMP.16.13601>
- [51] Karlová K, Strečka J and Lyra M L 2019 *Physical Review E* **100** 042127
- [52] Verkholyak T and Strečka J 2012 *Journal of Physics A: Mathematical and Theoretical* **45** 305001 URL <https://doi.org/10.1088/1751-8113/45/30/305001>
- [53] Strečka J, Rojas O, Verkholyak T and Lyra M L 2014 *Phys. Rev. E* **89**(2) 022143 URL <https://link.aps.org/doi/10.1103/PhysRevE.89.022143>
- [54] Strečka J, Rojas O, Verkholyak T and Lyra M L 2014 *Physical Review E* **89** 022143
- [55] Wootters W K 1998 *Phys. Rev. Lett.* **80**(10) 2245–2248 URL <https://link.aps.org/doi/10.1103/PhysRevLett.80.2245>
- [56] Karlová K and Strečka J 2020 *Acta Physica Polonica A* **137** 595–597
- [57] Quan H T and Cucchietti F M 2009 *Phys. Rev. E* **79**(3) 031101 URL <https://link.aps.org/doi/10.1103/PhysRevE.79.031101>
- [58] Rahaman S S, Sahoo S and Kumar M 2021 *Journal of Physics: Condensed Matter* **33** 265801 URL <https://doi.org/10.1088/1361-648x/abf882>
- [59] ER D 1975 *Journal of Computational Physics* **17** 87–94
- [60] Suzuki M 1985 *Physical Review B* **31** 2957